

A modified Anderson acceleration with sharp linear convergence rate predictions and application to incompressible flows

Yunhui He* Leo G Rebholz†

May 19, 2026

Abstract

In this work, we extend a modified Anderson acceleration proposed in [Y. He, arXiv:2603.25983, 2026] to accelerate the Picard iteration for the Navier-Stokes equations. In this variant of Anderson acceleration, named AAg, the nonlinear residual—rather than the standard fixed-point iteration residual—is used to define the associated least-squares problem. We establish a convergence analysis for this method with any depth that shows how AAg accelerates convergence through the gain of the optimization problem, and obtain a sharp prediction of its linear convergence rate (a feature that is not part of the known theory for classical Anderson acceleration). Additionally, motivated by this sharp convergence prediction, we introduce an adaptive strategy that automatically selects the depth parameter. Results of several numerical experiments are given that illustrate the new theory and also demonstrate the effectiveness of the proposed adaptive approach. Comparisons of AAg to usual AA and nonlinear GMRES are also provided.

Keywords. Anderson acceleration, nonlinear GMRES, least-squares problem, convergence analysis, Navier-Stokes equations, adaptive strategy

MSC. 65N22, 35Q30, 65N30, 65H10

1 Introduction

There has been a growing interest in the development and analysis of improved methods for solving nonlinear partial differential equations and nonlinear optimization problems arising from data science and machine learning. Recent achievements include significant advances in nonlinear acceleration [7, 16, 46, 54], nonlinear Krylov methods [8–10, 23, 26, 38, 56, 57], and others [34, 55].

Anderson acceleration (AA) [2] is one of the most popular nonlinear acceleration methods for improving fixed-point iterations. The framework of AA is presented in Algorithm 1, and its use is straightforward: the current iterate is updated by forming a linear combination of the current and m previous fixed-point iterates. At each step, the combination coefficients are obtained by solving a small least-squares problem based on the difference of the fixed-point iteration residuals, and hence the computational cost of solving the least-squares problem is typically negligible compared with evaluating a single fixed-point iteration. The depth m is a prescribed parameter, typically chosen to be small. Over the last 20 years, AA has been shown to accelerate and enable convergence on a very wide range of nonlinear (and linear) problems [1, 3, 6, 15, 18, 20, 39, 43, 51, 53, 54, 58, 60, 61], and many new variants have been proposed [4, 12, 17, 30, 48]. The behavior of AA at a single step is now at least generally understood, see [15, 40, 42, 44]. Some work has also

*Department of Mathematics, University of Houston, 3551 Cullen Blvd, Room 641, Houston, Texas 77204-3008, USA (yhe43@central.uh.edu).

†School of Mathematical and Statistical Sciences, Clemson University, Clemson, SC 29634, USA (rebholz@clemson.edu). This work was partially supported by Department of Energy grant DE-SC0025292.

been done regarding the choice of the depth parameter: A filtering strategy has been proposed in [41] to control the condition number of the least-squares matrix, which has been shown to be effective on a range of problems. Also, in [19, 40, 41], the authors propose using a small depth in the initial iterations and switching to a larger depth later, and show that this strategy enhances overall performance. However, there is no strong theoretical guidance on how to select the depth parameter. Several open questions remain for AA, regarding asymptotic convergence, how to best adaptively choose relaxation and depth parameters, why the extrapolation is done in that particular way, and why the least-squares problem is set up as it is.

Another nonlinear solver that has recently attracted considerable attention is the nonlinear GMRES (NGMRES) method [13, 14, 27, 38, 56], see Algorithm 2, and its new development [28, 31]. NGMRES is similar to AA, but has a different extrapolation and least-squares problem that uses the nonlinear residual instead of the fixed-point iteration residual to determine the combination coefficients. NGMRES has recently come under study, and understanding it may also provide insights into AA. For example, in [22], it is shown that under certain conditions, full depth NGMRES applied to the Richardson iteration for the linear problem is the same as classical GMRES. In the literature, it is well known for linear problems that full depth AA and classical GMRES are equivalent under certain conditions; see, for example [53]. NGMRES evolves as a nonlinear generalization of GMRES, and it minimizes the residual for linear systems. In [29], similar equivalence has been established for full depth NGMRES applied to preconditioned Richardson iteration and preconditioned GMRES.

In the original work of AA and NGMRES, the ℓ^2 norm is used for the least-squares problems, defined in Algorithms 1 and 2, respectively. However, recently, [24] and [32] show that an appropriate norm is needed in (3) and (5), which in some cases may not be ℓ^2 . The convergence analysis of AA-Picard for Navier-Stokes equations (NSE) and NGMRES-Picard have been done in [24] and [32], respectively. The work in [32] showed that in this setting, NGMRES analysis provides much sharper predictions of the linear convergence rates compared to existing AA theory. The key to the sharper predictions of NGMRES comes from using the nonlinear residual defined in (5), and thus it natural to ask whether the nonlinear residual can also be used to define the least-squares problem in AA method.

Consider solving $g(u) = 0$ with an iterative scheme defined by a fixed point function q , which might converge very slowly (or not at all). Recently, in [29], the author proposed a variant of AA, see Algorithm 3, referred to AAg(m) or simply AAg when the depth m is not specified. This new variant uses the nonlinear residual operator $g(\cdot)$ instead of the fixed-point iteration residual for the least-squares problem. To understand the AAg method, we present a brief introduction to the derivation of the least-squares problem defined in (6). The main idea is the same as the least-squares problem defined in (5) for NGMRES, and we aim to accelerate the sequence of iterates generated by $q(\cdot)$. Writing $u_j^q = q(u_j)$, the new update is based on the linear approximation of the nonlinear operator g in the space

$$u_k^q + \text{span}\{u_k^q - u_{k-1}^q, u_k^q - u_{k-2}^q, \dots, u_k^q - u_{k-m}^q\}.$$

We approximate g near u_k^q by the Taylor expansion

$$\begin{aligned} g(u_k^q + \sum_{i=1}^m \xi_i (u_k^q - u_{k-i}^q)) &\approx g(u_k^q) + \sum_{i=1}^m \frac{\partial g}{\partial u} \Big|_{u_k^q} (u_k^q - u_{k-i}^q) \\ &\approx g(u_k^q) + \sum_{i=1}^m (g(u_k^q) - g(u_{k-i}^q)). \end{aligned} \quad (1)$$

If we replace m by $m_k = \{m, k\}$ and set the new update as $u_{k+1} = u_k^q + \sum_{i=1}^{m_k} \xi_i (u_k^q - u_{k-i}^q)$, we obtain Algorithm 3.

In [29], the author studied the properties of AAg only for linear problems, with no exploration of the nonlinear cases. We are interested herein in exploring the convergence analysis and performance for the new variant AAg for a nonlinear problem, in particular by applying AAg to the Picard iteration for solving the NSE. Moreover, we will compare the performance of AAg with the well-known AA and NGMRES methods.

Specifically, in this work we provide a convergence analysis for AAg, and show that sharp predictions of the linear convergence rate are attainable using the norm of the range of g in the optimization problem. We

compare AA, AAg, and NGMRES for accelerating the Picard iteration for the NSE. We observe that AA and AAg perform similarly, and are both slightly better than NGMRES for the test problems considered here. Based on the sharp convergence predictions of AAg, we develop an adaptive strategy for choosing the depth parameter used in AAg. Numerical experiments demonstrate the effectiveness of this approach, showing substantial improvements in the iteration counts of adaptive AAg.

We now state Algorithms 1, 2 and 3. The notation $\|\cdot\|_q$ denotes the norm of the range space of q and $\|\cdot\|_g$ denotes the norm of the range space of g . In practice, often ℓ^2 is chosen, but in certain settings using the appropriate function space norms to match the theories may provide better results [24, 32].

Algorithm 1 AA(m): Anderson acceleration with depth m

- 1: **input:** u_0 , fixed-point operator $q(\cdot)$, and $m \geq 0$ with $m \in \mathbb{N}$
- 2: **for** $k = 0, 1, \dots$ until convergence **do**
- 3: compute

$$u_{k+1} = q(u_k) + \sum_{i=1}^{m_k} \tau_i^{(k)} (q(u_k) - q(u_{k-i})), \quad (2)$$

where $m_k = \min\{k, m\}$ and $\tau^{(k)} = (\tau_1^{(k)}, \dots, \tau_{m_k}^{(k)})$ is obtained by solving the least-squares problem

$$\min_{\tau^{(k)}} \left\| w(u_k) + \sum_{i=1}^{m_k} \tau_i^{(k)} (w(u_k) - w(u_{k-i})) \right\|_q^2, \quad (3)$$

where $w_{k+1} = w(u_k) = q(u_k) - u_k$ is the fixed-point iteration residual.

- 4: **end for**
 - 5: **output:** u_{k+1}
-

Algorithm 2 NGMRES(m): Nonlinear GMRES with depth m for solving $g(u) = 0$

- 1: **input:** u_0 , fixed-point operator $q(\cdot)$, and $m \geq 0$ with $m \in \mathbb{N}$
- 2: **for** $k = 0, 1, \dots$ until convergence **do**
- 3: compute

$$u_{k+1} = q(u_k) + \sum_{i=0}^{m_k} \beta_i^{(k)} (q(u_k) - u_{k-i}), \quad (4)$$

where $m_k = \min\{k, m\}$ and $\beta^{(k)} = (\beta_0^{(k)}, \beta_1^{(k)}, \dots, \beta_{m_k}^{(k)})$ is obtained by solving the least-squares problem

$$\min_{\beta^{(k)}} \left\| g(q(u_k)) + \sum_{i=0}^{m_k} \beta_i^{(k)} (g(q(u_k)) - g(u_{k-i})) \right\|_g^2. \quad (5)$$

- 4: **end for**
 - 5: **output:** u_{k+1}
-

Algorithm 3 AAg(m): Anderson acceleration with g -norm for solving $g(u) = 0$

- 1: **input:** u_0 , fixed-point operator $q(\cdot)$, and $m \geq 0$ with $m \in \mathbb{N}$
- 2: **for** $k = 0, 1, \dots$ until convergence **do**
- 3: compute

$$u_{k+1} = q(u_k) + \sum_{i=1}^{m_k} \xi_i^{(k)} (q(u_k) - q(u_{k-i})),$$

where $m_k = \min\{k, m\}$ and $\xi^{(k)} = (\xi_1^{(k)}, \dots, \xi_{m_k}^{(k)})$ is obtained by solving the least-squares problem

$$\min_{\xi^{(k)}} \left\| g(q(u_k)) + \sum_{i=1}^{m_k} \xi_i^{(k)} (g(q(u_k)) - g(q(u_{k-i}))) \right\|_g^2. \quad (6)$$

- 4: **end for**
 - 5: **output:** u_{k+1}
-

The remainder of this work is organized as follows. In section 2, we provide a brief introduction to the NSE, its associated Picard iteration, and various properties. In section 3, we present a convergence analysis for AAg with depth one and then with general depth. Numerical results for 2D channel flow past a block, 3D driven cavity, and a 3D stenotic artery model are presented in section 4, where we show the performance of AAg, AA and NGMRES. Finally, we draw conclusions in section 5.

2 Notation and Preliminaries

We consider the domain $\Omega \subset \mathbb{R}^d$ ($d=2$ or 3) to be an open connected set. We use the notation (\cdot, \cdot) and $\|\cdot\|$ for the $L^2(\Omega)$ inner product and norm, respectively. Other norms will be labeled with subscripts.

The natural velocity and pressure spaces for the NSE are defined by

$$\begin{aligned} X &:= \{v \in H^1(\Omega) : v = 0 \text{ on } \partial\Omega\}, \\ Q &:= \{q \in L^2(\Omega) : \int_{\Omega} q \, dx = 0\}, \end{aligned}$$

and the divergence-free velocity space is given by

$$V := \{v \in X : (\nabla \cdot v, q) = 0 \, \forall q \in Q\}.$$

The dual space $X' = H^{-1}(\Omega)$, with norm $\|\cdot\|_{-1}$. The dual space of V is denoted by V' , and uses norm $\|\cdot\|_{V'}$. We will abuse notation slightly and use (\cdot, \cdot) also for dual pairings of V and X with their dual spaces.

We recall from [36] some well-known properties for the nonlinear form $(v \cdot \nabla w, \chi)$. First, if $v \in V$ and $w \in X$, then

$$(v \cdot \nabla w, w) = 0.$$

Additionally, for $v, w, \chi \in V$,

$$(v \cdot \nabla w, \chi) \leq M \|\nabla v\| \|\nabla w\| \|\nabla \chi\|, \quad (7)$$

$$\|v \cdot \nabla w\|_{V'} \leq M \|\nabla v\| \|\nabla w\|. \quad (8)$$

This paper works primarily in the space V and its dual space. The above results, and the rest of the results throughout this paper, would be nearly identical if we worked in the discretely divergence-free subspace V_h from an inf-sup stable velocity-pressure pair $(X_h, Q_h) \subset (X, Q)$, provided that a skew-symmetric form of the nonlinearity is used if divergence-free finite elements were not used, e.g. skew-symmetric form, rotational form or EMAC [11, 35].

2.1 NSE preliminaries

The steady NSE are given by

$$\begin{cases} -\nu\Delta u + u \cdot \nabla u + \nabla p = f & \text{in } \Omega, \\ \nabla \cdot u = 0 & \text{in } \Omega, \\ u = 0 & \text{on } \partial\Omega, \end{cases} \quad (9)$$

where u is the velocity and p is the pressure, $\nu > 0$ is the kinematic viscosity and f is a given external forcing. The Reynolds number $Re = O(\frac{1}{\nu})$ is another physical constant often used to describe the complexity of a flow. We consider the system (9) equipped with homogeneous Dirichlet boundary conditions for simplicity of analysis, but our results are extendable to nonhomogeneous mixed Dirichlet/Neumann boundary conditions and to a time dependent NSE scheme at a fixed time step.

The weak form of (9) is: Find $u \in V$ such that

$$\nu(\nabla u, \nabla v) + (u \cdot \nabla u, v) = (f, v) \quad \forall v \in V. \quad (10)$$

It is known that solutions to (10) exist for any $\nu > 0$ and $f \in H^{-1}(\Omega)$ [36], and are bounded by

$$\|\nabla u\| \leq \nu^{-1} \|f\|_{-1}. \quad (11)$$

Under a small data sufficient condition $\kappa := M\nu^{-2} \|f\|_{H^{-1}} < 1$, solutions are known to be unique [21, 36, 49]. However, for κ large enough, (10) can have multiple solutions [36].

2.2 Picard and nonlinear residual preliminaries

The Picard iteration for solving (10) is: Given $u_k \in V$, find $q(u_k) \in V$ such that

$$\nu(\nabla q(u_k), \nabla v) + (u_k \cdot \nabla q(u_k), v) = (f, v) \quad \forall v \in V. \quad (12)$$

It is shown in [44] that the solution operator $q : V \rightarrow V$ associated with (12) is well-defined and is uniformly bounded:

$$\|\nabla q(u_k)\| \leq \nu^{-1} \|f\|_{-1}. \quad (13)$$

Thus, we can define the fixed-point Picard iteration as $u_{k+1} = q(u_k)$. In AAg (and AA), Picard is used as a first step and then a second step is used as a type of extrapolation or correct. Thus we will also use the notation $\tilde{u}_{k+1} = q(u_k)$ for a Picard iterate in that context. The Picard fixed-point iteration residual satisfies [21]

$$\|\nabla(q(u_k) - u_k)\| \leq \kappa \|\nabla(q(u_{k-1}) - u_{k-1})\|. \quad (14)$$

Equation (14) implies that $\kappa < 1$ yields a contractive Picard iteration that will converge linearly with rate κ to the unique weak solution. For sufficiently large κ , it is known that the Picard iteration will diverge [42]. Herein, we assume that the Picard iteration is contractive by assuming that $\kappa < 1$. This assumption is needed in our analysis for the higher order terms, although in our numerical tests we use $\kappa \gg 1$, i.e. far above the range where Picard is contractive.

We also consider the NSE nonlinear residual operator, which is defined by $g : V \rightarrow V'$ satisfying for all $v \in V$ and $\chi \in V$,

$$(g(v), \chi) = \nu(\nabla v, \nabla \chi) + (v \cdot \nabla v, \chi) - (f, \chi). \quad (15)$$

The V' norm of $g(v)$ is thus defined by

$$\|g(v)\|_{V'} = \max_{0 \neq \chi \in V} \frac{(g(v), \chi)}{\|\nabla \chi\|}. \quad (16)$$

Due to $v \in V$, the $v \cdot \nabla v$ term is not in $L^2(\Omega)$, and thus V' is the appropriate norm for measuring $g(v)$.

For notational simplicity, it is very helpful in our analysis to denote

$$\tilde{u}_{k+1} := q(u_k).$$

It is also useful in our analysis to define the Picard fixed-point residual by

$$w_{k+1} = q(u_k) - u_k = \tilde{u}_{k+1} - u_k.$$

The following bounds were proven in [32] regarding the Picard fixed point residual and the NSE nonlinear residual:

$$\|\nabla w_{k+1}\| \leq \nu^{-1} \|g(u_k)\|_{V'}, \quad (17)$$

$$\|g(\tilde{u}_{k+1})\|_{V'} \leq \kappa \|g(u_k)\|_{V'}. \quad (18)$$

Define $e_k = u_k - u_{k-1}$. The following result is proven in [32] relating the nonlinear and fixed-point residuals.

Lemma 2.1. *For any depth $m > 0$ and assuming $\kappa < 1$, the difference between successive iterates satisfies*

$$\|\nabla e_k\| \leq \frac{\nu^{-1}}{1 - \kappa} (\|g(u_k)\|_{V'} + \|g(u_{k-1})\|_{V'}). \quad (19)$$

Proof. This is proven in [32]. □

It will also be useful to define the quantity $\tilde{e}_k = \tilde{u}_k - \tilde{u}_{k-1}$. Since for all $v \in V$,

$$\begin{aligned} \nu(\nabla \tilde{u}_k, \nabla v) + (u_{k-1} \cdot \nabla \tilde{u}_k, v) &= (f, v), \\ \nu(\nabla \tilde{u}_{k-1}, \nabla v) + (u_{k-2} \cdot \nabla \tilde{u}_{k-1}, v) &= (f, v), \end{aligned}$$

we have that

$$\nu(\nabla \tilde{e}_k, \nabla v) + (e_{k-1} \cdot \nabla \tilde{u}_k, v) + (u_{k-2} \cdot \nabla \tilde{e}_k, v) = 0.$$

Hence with $v = e_k$, using (7), (13) and the definition of κ we get that

$$\|\nabla \tilde{e}_k\| \leq M\nu^{-1} \|\nabla e_{k-1}\| \|\nabla \tilde{u}_k\| \implies \|\nabla \tilde{e}_k\| \leq \kappa \|\nabla e_{k-1}\|. \quad (20)$$

This will be useful bound below.

3 Convergence analysis of AAg

We now consider convergence analysis of AAg applied to the Picard iteration for the NSE. Hence in what follows, g is the nonlinear residual defined by (15), and q is the NSE Picard iteration defined by (12). For convenience in our analysis, we rewrite AAg, presented in 3, as Algorithm 4, which expresses the combination coefficients in an equivalent constraint-based format. For simplicity, since we do a single step analysis, we omit the superscript that appears in the coefficients $\alpha_{k+1-i}^{(k)}$ in the following analysis.

Algorithm 4 AAg(m): Alternative format of Anderson acceleration with g-norm for solving $g(u) = 0$

- 1: **input:** u_0 , fixed-point operator $q(\cdot)$, and $m \geq 0$ with $m \in \mathbb{N}$
- 2: **for** $k = 0, 1, \dots$ until convergence **do**
- 3: compute

$$u_{k+1} = \sum_{i=0}^{m_k} \alpha_{k+1-i}^{(k)} q(u_{k-i}),$$

where $m_k = \min\{k, m\}$ and $\{\alpha_{k+1-i}^{(k)}\}_{i=0}^{m_k}$ are obtained by solving the least-squares problem

$$\min_{\sum_{i=k-m_k+1}^{k+1} \alpha_i^{(k)} = 1} \left\| \alpha_{k-m_k+1}^{(k)} g(q(u_{k-m_k})) + \alpha_{k-m_k+2}^{(k)} g(q(u_{k-m_k+1})) \cdots + \alpha_{k+1}^{(k)} g(q(u_k)) \right\|_{V'}^2. \quad (21)$$

- 4: **end for**
 - 5: **output:** u_{k+1}
-

We now prove convergence estimates for AAg. Under the assumption that $\kappa < 1$ so that the Picard iteration is contractive, we prove how AAg accelerates convergence by scaling the linear convergence rate by the gain of the optimization problem, which is defined by

$$\theta_{k+1} = \frac{\|\sum_{j=k-m_{k+1}+1}^{k+1} \alpha_j g(\tilde{u}_j)\|_{V'}}{\|g(\tilde{u}_{k+1})\|_{V'}}.$$

The numerator comes from the optimization problem, and the denominator comes from not using acceleration but just the Picard iteration, which is equivalent to picking the parameters $[1, 0, \dots, 0]$. Since $[1, 0, \dots, 0]$ is in the admissible set of parameters, we have that $\theta \leq 1$, but $\theta = 1$ is very unlikely.

Further, we give an estimate of the linear convergence rate of $\|g(u_k)\|_{V'}$ at each iteration:

$$\gamma_{k+1} = \frac{\|\sum_{j=k-m_k+1}^{k+1} \alpha_j g(\tilde{u}_j)\|_{V'}}{\|g(u_k)\|_{V'}}.$$

Our numerical tests show γ_{k+1} gives a very sharp estimate of the contraction ratio at each iteration, once the residual is moderately reduced so the higher order terms become negligible. We also show in our numerical tests that γ_{k+1} can be used to adaptively choose the depth m at each step of AAg.

The AAg convergence theory for general m is long and somewhat tedious, and so we first prove the result for $m = 1$ so that reader can have some intuition of the proof structure before we prove the general m result.

3.1 AAg convergence for $m = 1$

We begin by establishing two identities for the $m = 1$ case. Recall that

$$u_{k+1} = \alpha_{k+1} \tilde{u}_{k+1} + \alpha_k \tilde{u}_k,$$

where $\alpha_{k+1} + \alpha_k = 1$. First, expanding $u_{k+1} - \tilde{u}_{k+1}$ and using the definition of u_{k+1} yields

$$u_{k+1} - \tilde{u}_{k+1} = -(1 - \alpha_{k+1}) \tilde{u}_{k+1} + \alpha_k \tilde{u}_k = -\alpha_k \tilde{e}_{k+1}. \quad (22)$$

Similarly, expanding $u_{k+1} - \tilde{u}_k$ gives

$$u_{k+1} - \tilde{u}_k = \alpha_{k+1} \tilde{u}_{k+1} + (\alpha_k - 1) \tilde{u}_k = \alpha_{k+1} \tilde{e}_{k+1}. \quad (23)$$

Theorem 3.1. *AAg with $m = 1$ presented in Algorithm 4. If $\kappa < 1$, then for $k > 1$,*

$$\begin{aligned} \|g(u_{k+1})\|_{V'} &\leq \theta_{k+1} \kappa \|g(u_k)\|_{V'} + \frac{2\bar{\alpha}^2 \kappa^2}{\nu^2 (1 - \kappa)^2} (\|g(u_k)\|_{V'}^2 + \|g(u_{k-1})\|_{V'}^2), \\ \|g(u_{k+1})\|_{V'} &\leq \gamma_{k+1} \|g(u_k)\|_{V'} + \frac{2\bar{\alpha}^2 \kappa^2}{\nu^2 (1 - \kappa)^2} (\|g(u_k)\|_{V'}^2 + \|g(u_{k-1})\|_{V'}^2). \end{aligned}$$

Remark 3.1. *Since κ is the linear convergence rate of Picard iteration, the quantity θ_{k+1} represents the convergence acceleration provided by AAg. Since in practice κ is hard to know precisely, the quantity γ_{k+1} represents a sharper estimate of the linear convergence rate at each iteration. Note that it is consistent with (1) that the $(k + 1)$ st residual is bounded by the linear part of k th residual and high-order part of k th and $(k - 1)$ st residuals.*

Proof. To reduce on notation, the following two equality strings will be understood to hold in the weak sense when tested with an arbitrary function from V .

We begin the proof by developing an identity for $g(u_{k+1})$ through expanding u_{k+1} using its definition and that $\alpha_k + \alpha_{k+1} = 1$ to obtain

$$\begin{aligned} g(u_{k+1}) &= u_{k+1} \cdot \nabla u_{k+1} - \nu \Delta u_{k+1} - f \\ &= \alpha_{k+1} (\tilde{u}_{k+1} \cdot \nabla u_{k+1} - \nu \Delta \tilde{u}_{k+1} - f) + \alpha_k (\tilde{u}_k \cdot \nabla u_{k+1} - \nu \Delta \tilde{u}_k - f) \\ &= \alpha_{k+1} (g(\tilde{u}_{k+1}) + \tilde{u}_{k+1} \cdot \nabla (u_{k+1} - \tilde{u}_{k+1})) + \alpha_k (g(\tilde{u}_k) + \tilde{u}_k \cdot \nabla (u_{k+1} - \tilde{u}_k)). \end{aligned}$$

Next, regrouping terms and using (22)-(23), we get that

$$\begin{aligned} g(u_{k+1}) &= (\alpha_{k+1}g(\tilde{u}_{k+1}) + \alpha_k g(\tilde{u}_k)) + \alpha_{k+1}\tilde{u}_{k+1} \cdot \nabla(u_{k+1} - \tilde{u}_{k+1}) + \alpha_k \tilde{u}_k \cdot \nabla(u_{k+1} - \tilde{u}_k) \\ &= (\alpha_{k+1}g(\tilde{u}_{k+1}) + \alpha_k g(\tilde{u}_k)) - \alpha_{k+1}\alpha_k \tilde{u}_{k+1} \cdot \nabla \tilde{e}_{k+1} + \alpha_k \alpha_{k+1} \tilde{u}_k \cdot \nabla \tilde{e}_{k+1} \\ &= (\alpha_{k+1}g(\tilde{u}_{k+1}) + \alpha_k g(\tilde{u}_k)) - \alpha_k \alpha_{k+1} \tilde{e}_{k+1} \cdot \nabla \tilde{e}_{k+1}. \end{aligned}$$

Taking V' norms of both sides, using the triangle inequality, the bound on α_j 's and (20) gives

$$\begin{aligned} \|g(u_{k+1})\|_{V'} &\leq \|\alpha_{k+1}g(\tilde{u}_{k+1}) + \alpha_k g(\tilde{u}_k)\|_{V'} + \bar{\alpha}^2 \|\nabla \tilde{e}_{k+1}\|^2 \\ &\leq \|\alpha_{k+1}g(\tilde{u}_{k+1}) + \alpha_k g(\tilde{u}_k)\|_{V'} + \bar{\alpha}^2 \kappa^2 \|\nabla e_k\|^2. \end{aligned}$$

Finally, using (19), we obtain the estimate

$$\|g(u_{k+1})\|_{V'} \leq \|\alpha_{k+1}g(\tilde{u}_{k+1}) + \alpha_k g(\tilde{u}_k)\|_{V'} + \frac{\bar{\alpha}^2 \kappa^2}{\nu^2(1-\kappa)^2} (\|g(u_k)\|_{V'} + \|g(u_{k-1})\|_{V'})^2.$$

From here, inserting the definitions of θ_{k+1} and γ_{k+1} for the lower order term along with Young's inequality for the higher order terms gives the two estimates

$$\begin{aligned} \|g(u_{k+1})\|_{V'} &\leq \theta_{k+1} \|g(\tilde{u}_{k+1})\|_{V'} + \frac{\bar{\alpha}^2 \kappa^2}{\nu^2(1-\kappa)^2} (\|g(u_k)\|_{V'} + \|g(u_{k-1})\|_{V'})^2, \\ \|g(u_{k+1})\|_{V'} &\leq \gamma_{k+1} \|g(u_k)\|_{V'} + \frac{\bar{\alpha}^2 \kappa^2}{\nu^2(1-\kappa)^2} (\|g(u_k)\|_{V'} + \|g(u_{k-1})\|_{V'})^2. \end{aligned}$$

Lastly, using Lemma 2.1 from [32] which gives that $\|g(\tilde{u}_{k+1})\|_{V'} \leq \kappa g(u_k)\|_{V'}$, finishes the proof. \square

3.2 AAg convergence for general m

We now prove a convergence estimate for AAg in the case of general m . The strategy is the same as for the $m = 1$ case: first we write $g(u_{k+1})$ in terms of $\sum_{j=k-m+1}^{k+1} \alpha_j g(\tilde{u}_j)$, and then bound the remainder terms. We first establish a lemma useful for the main theorem to follow.

Lemma 3.1. *Consider AAg with $m > 1$ presented in Algorithm 4. For $k > m$, the following identities hold:*

$$\begin{aligned} u_{k+1} - \tilde{u}_{k+1} &= -(1 - \alpha_{k+1})\tilde{e}_{k+1} - (1 - \alpha_{k+1} - \alpha_k)\tilde{e}_k - \dots - \alpha_{k-m+1}\tilde{e}_{k-m+2}, \\ u_{k+1} - \tilde{u}_k &= \alpha_{k+1}\tilde{e}_{k+1} - (1 - \alpha_{k+1} - \alpha_k)\tilde{e}_k - (1 - \alpha_{k+1} - \alpha_k - \alpha_{k-1})\tilde{e}_{k-1} \\ &\quad - \dots - \alpha_{k-m+1}\tilde{e}_{k-m+2}, \\ u_{k+1} - \tilde{u}_{k-1} &= \alpha_{k+1}\tilde{e}_{k+1} + (\alpha_{k+1} + \alpha_k)\tilde{e}_k - (1 - \alpha_{k+1} - \alpha_k - \alpha_{k-1})\tilde{e}_{k-1} \\ &\quad - \dots - \alpha_{k-m+1}\tilde{e}_{k-m+2}, \\ \text{for } j < k-1: \quad u_{k+1} - \tilde{u}_j &= \alpha_{k+1}\tilde{e}_{k+1} + (\alpha_{k+1} + \alpha_k)\tilde{e}_k + \dots + (\alpha_{k+1} + \alpha_k + \dots + \alpha_{j+1})\tilde{e}_{j+1} \\ &\quad (1 - \alpha_{k+1} - \dots - \alpha_j)\tilde{e}_j - \dots - \alpha_{k-m+1}\tilde{e}_{k-m+2}. \end{aligned}$$

Proof. This proof follows from identities, and is given in the Appendix. \square

The general m AAg convergence theorem can now be stated as follows.

Theorem 3.2. *Consider AAg with $m > 1$ presented in Algorithm 4. If $\kappa < 1$, then for $k > m$:*

$$\|g(u_{k+1})\|_{V'} \leq \min\{\theta_{k+1}\kappa, \gamma_{k+1}\} \|g(u_k)\|_{V'} + 4M(m+1)m^3 \bar{\alpha}^2 \frac{\kappa^2}{\nu^2(1-\kappa)^2} \sum_{i=0}^m \|g(u_{k-i})\|_{V'}^2.$$

Remark 3.2. *For $1 < k \leq m$, the result in Theorem 3.2 holds after replacing m with $m_k = \min\{m, k\}$ on the right-hand side on the above inequality.*

Remark 3.3. Since κ is the linear convergence rate of Picard, the quantity θ_{k+1} represents the convergence acceleration provided by AAg. Since in practice κ is hard to know precisely, the quantity γ_{k+1} represents a sharper estimate of the linear convergence rate at each iteration. We show in our numerical tests that γ_{k+1} is a sharp estimate of the linear convergence rate, and indeed sharp enough that it can be used to develop strategies for adaptive m at each iteration.

Proof. Note that for $k > m$, $m_k = \min\{m, k\} = m$. We establish using a long string of identities in (28) and (29) in the Appendix that

$$g(u_{k+1}) = \alpha_{k+1}g(\tilde{u}_{k+1}) + \alpha_k g(\tilde{u}_k) + \dots + \alpha_{k-m+1}g(\tilde{u}_{k-m+1}) + \sum_{j=k-m+2}^{k+1} \sum_{i=j}^{k+1} \alpha_i \tilde{e}_j \cdot \nabla(u_{k+1} - \tilde{u}_i), \quad (24)$$

where equality is meant in the weak sense, i.e. equality holds when the equation is tested with an arbitrary function from V . Using Lemma 3.1, up to coefficients all higher order terms take the form $\tilde{e}_j \cdot \nabla \tilde{e}_i$. Thus using (8), (20) and (19), we have that

$$\begin{aligned} & \sum_{j=k-m+2}^{k+1} \sum_{i=j}^{k+1} \alpha_i \tilde{e}_j \cdot \nabla(u_{k+1} - \tilde{u}_i) \\ & \leq 4M(m+1)m\bar{\alpha}^2 \sum_{i,j=k-m+2}^{k+1} \|\nabla \tilde{e}_j\| \|\nabla \tilde{e}_i\| \\ & \leq 4M(m+1)m^3 \frac{\bar{\alpha}^2 \kappa^2}{\nu^2(1-\kappa)^2} \sum_{j=k-m}^k \|g(u_j)\|_{V'}^2. \end{aligned} \quad (25)$$

Now taking V' norms of (24) and using (25) provides

$$\begin{aligned} \|g(u_{k+1})\|_{V'} & \leq \|\alpha_{k+1}g(\tilde{u}_{k+1}) + \alpha_k g(\tilde{u}_k) + \dots + \alpha_{k-m+1}g(\tilde{u}_{k-m+1})\|_{V'} \\ & \quad + 4M(m+1)m^3 \bar{\alpha}^2 \frac{\kappa^2}{\nu^2(1-\kappa)^2} \sum_{j=k-m}^k \|g(u_j)\|_{V'}^2. \end{aligned}$$

Now using the definitions of θ_{k+1} and γ_{k+1} , we obtain

$$\|g(u_{k+1})\|_{V'} \leq \theta_{k+1} \|g(\tilde{u}_{k+1})\|_{V'} + 4M(m+1)m^3 \bar{\alpha}^2 \frac{\kappa^2}{\nu^2(1-\kappa)^2} \left(\|g(u_k)\|_{V'}^2 + \|g(u_{k-1})\|_{V'}^2 + \dots + \|g(u_{k-m})\|_{V'}^2 \right), \quad (26)$$

and

$$\|g(u_{k+1})\|_{V'} \leq \gamma_{k+1} \|g(u_k)\|_{V'} + 4M(m+1)m^3 \bar{\alpha}^2 \frac{\kappa^2}{\nu^2(1-\kappa)^2} \left(\|g(u_k)\|_{V'}^2 + \|g(u_{k-1})\|_{V'}^2 + \dots + \|g(u_{k-m})\|_{V'}^2 \right).$$

Finally, using (18) in (26) completes the proof. \square

4 Numerical Experiments

We now present results of several numerical tests to illustrate the AAg theory, compare convergence behavior of AAg, AA and NGMRES, and discuss an adaptive depth strategy for AAg. The theorems presented in this work use the V' norm, and we compute this norm in our computations using

$$\|\phi_h\|_{V'}^2 := (\phi_h, A_h^{-1} \phi_h),$$

where A_h is the discrete Stokes operator with boundary conditions enforced in the matrix (i.e. remove degrees of freedom (dof) associated with Dirichlet velocity boundary conditions). As shown in [32] for the NGMRES method, using this norm in the optimization problem (instead of the more commonly used ℓ^2 norm) is important for ensuring that the computations behave as the theory predicts, especially in 3D. More specifically, if we instead use the ℓ^2 norm, then 2D results are similar as what is shown below, but 3D results are much worse. In a similar vein, the optimization norm used in our tests for NGMRES is V' (to agree with the theory in [32]), and the optimization norm used for AA is H_0^1 (to agree with theory in [24, 40, 44]).

In this section, we first present the convergence results for AAg and γ_k , then compare the performance of AAg, AA and NGMRES, and finally propose an adaptive depth strategy for AAg-Picard. The adaptive depth strategy greatly improves the performance of the AA method.

4.1 Test problem setup

We now give descriptions of the test problems used in our numerical experiment: 2D channel flow past a block, 3D driven cavity, and a 3D stenotic artery model.

4.1.1 Channel flow past a cylinder

For our first test problem, we use the classical 2D channel flow past a block benchmark from e.g. [25, 45, 47, 52]. The domain is a 2.2×0.41 rectangular channel with a square of side length 0.1 centered at $(0.2, 0.2)$. No-slip velocity is enforced on the walls and block, and at the inflow and outflow we enforce

$$u(0, y) = \begin{pmatrix} \frac{6}{0.41^2}y(0.41 - y) \\ 0 \end{pmatrix}. \quad (27)$$

There is no external forcing ($f = 0$), and we use varying $Re = \frac{UL}{\nu} = 100, 150$ and 200 , which are calculated using length scale $L = 0.1$ as the block width, and $U = 1$. We note that the NSE with $Re > 50$ is known to produce periodic-in-time solutions [25, 37], but we are solving for steady state solutions at these Re (recall steady solutions exist for any Re [36]). A solution from our computations with $Re=100$ is shown in Figure 1.

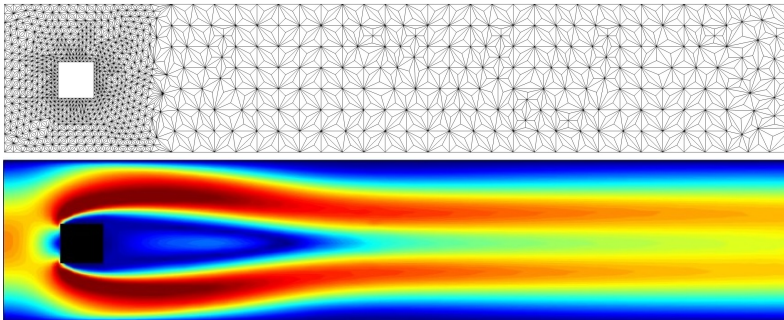


Figure 1: Shown above is a sample mesh for 2D channel flow past a block (top) and $Re=100$ solution shown as speed contours.

For the discretization, (P_2, P_1^{disc}) Scott-Vogelius (SV) elements are used on barycenter refined Delaunay meshes of the domain. Computations were done on several meshes, with results nearly identical across meshes (which is expected, as the convergence results are mesh independent and other AA and NGMRES tests have always shown mesh independence [32, 42]). The mesh used for the results below provided 120K velocity and 89K pressure dof. Figure 1 shows a coarse mesh of the domain, significantly coarser than what is used in our tests. The nonlinear solver tolerance was taken to be 10^{-8} in the V' norm, and the linear solves for these 2D tests used a direct solver.

4.1.2 3D driven cavity

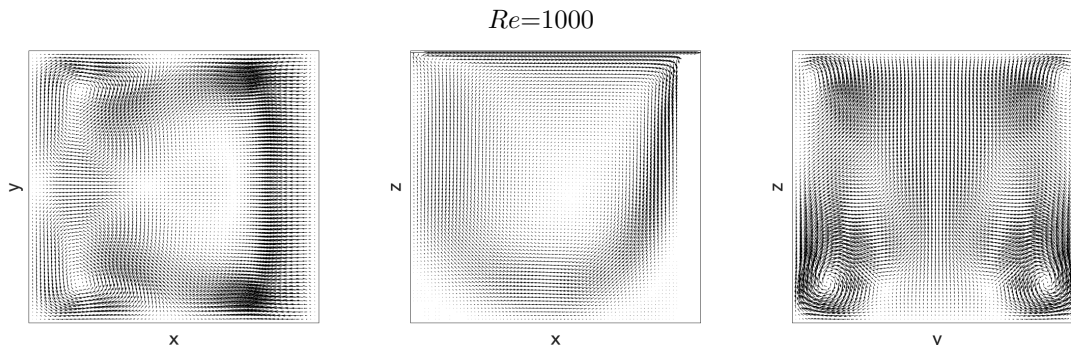


Figure 2: The plot above shows the $Re=1000$ 3D driven cavity velocity solution displayed as midsliceplanes of velocity.

The 3D driven cavity is used for our second benchmark test. This problem is analogous to the well studied 2D driven cavity, where $f = 0$, $\Omega = (0, 1)^3$, and homogeneous Dirichlet boundary conditions for velocity are enforced on the walls but $[1, 0, 0]^T$ is enforced on the ‘lid’. We compute with $Re = \frac{1}{\nu} = 400$ and 1000, and midsliceplane velocity vector solutions for $Re=1000$ are shown in Figure 2.

The mesh is constructed as follows: first we create a \mathcal{M}^3 grid of boxes from Chebychev points on $[0, 1]$, then refine each box into 6 tetrahedra, and finally barycenter refine each of those tetrahedra into 4 tetrahedra. Computations used $\mathcal{M} = 11$ and 13, which provided 796K and 1.3M total dof, respectively, when equipped with (P_3, P_2^{disc}) SV elements, and no difference was observed for the convergence or solutions on the two meshes. Hence results are shown only for the fine mesh below. Our computed solutions were found to match the literature well [59], see Figure 2. The nonlinear solver tolerance was 10^{-7} in the V' norm. The linear solves used an augmented Lagrangian preconditioning essentially following [5,33] (using grad-div stabilization and preconditioning the Schur complement with the pressure mass matrix) with GMRES as the outer solver and direct inner solves of the velocity submatrix. The outer linear solver tolerance was set as 10^{-11} , and convergence was generally reached within 3 to 5 iterations.

4.1.3 Flow in a 3D stenotic artery model

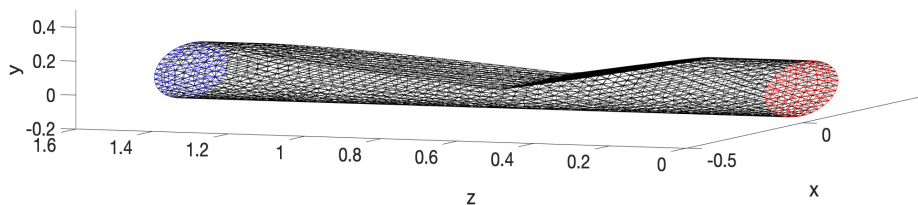


Figure 3: Shown above is the artery mesh (before the barycenter refinement is applied) restricted to the surface.

For our last test problem, we use the stenotic artery model from [50], and note that this application benchmark is not non-dimensional in the literature, and has length units given in cm and time units in seconds. The vessel domain is created from a 3D deformed cylinder with diameter $d = 0.16$ and length

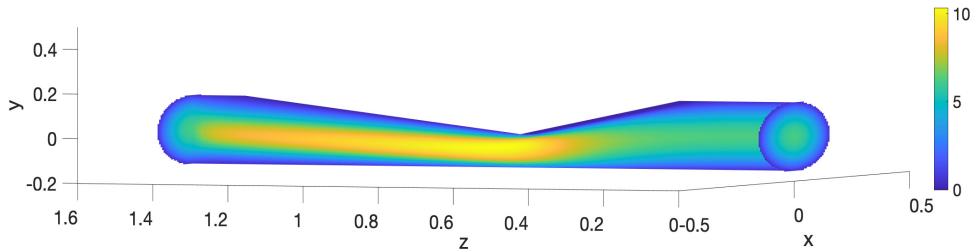


Figure 4: Shown above is speed contour slices for the $\nu = \frac{1}{500}$ solution.

$l = 1.6$. We enforce no-slip velocity on the artery walls, and parabolic and outflow using a maximum velocity at the vessel center of 6.22. The viscosity is taken to be $\nu = 0.002$, and no forcing is used.

The domain is discretized first from a regular tetrahedralization (thanks to the authors of [50] for providing the mesh!), which is shown as a surface mesh in Figure 3. This mesh is then barycenter refined, which gives 52,912 total tetrahedra, and is then equipped with (P_3, P_2^{disc}) SV elements, yielding 1.33M total dof. A plot of the solution found on this mesh using AAg-Picard is shown in Figure 4. The same linear solver used for the 3D driven cavity is used on this problem. Due to the mesh aspect ratio together with a linear solver tolerance of 10^{-10} , $\|\nabla \cdot u_k\|$ could only converge to about 10^{-5} , which limited convergence of the nonlinear solver since then u_k convergence in the H_0^1 norm is automatically limited (since the elements are divergence-free elements). Thus we chose a convergence tolerance of 10^{-5} in the V' norm for this problem.

4.2 Tests for AAg convergence and γ_k

We now consider convergence behavior of AAg-Picard on the 2D channel flow past a block with $Re=100$ and 150, the 3D driven cavity with $Re=400$ and 1000, and the 3D stenotic artery model. We compute convergence as the nonlinear residual in the V' norm $\|g(u_k)\|_{V'}$ (to match theory), and the Picard residual in the H_0^1 norm $\|\nabla(g(u_k) - u_k)\|$ (to match the usual Picard convergence theory [21, 49] and AA-Picard theory [42, 44]). We observe very similar convergence behavior from these norms in all tests, although the actual values of the two norms are typically off by a constant. Convergence of these residuals measured in ℓ^2 norms also show similar convergence behavior (plots omitted). We also compute γ_k and plot it along with the linear convergence ratio $\frac{\|g(u_k)\|_{V'}}{\|g(u_{k-1})\|_{V'}}$, to test the accuracy of γ_k as the linear convergence rate predictor.

Results are shown in Figure 5, for AAg-Picard with varying depths (depth ∞ means $m = k-1$ at iteration k for AAg), along with usual Picard. First we note that the first and second columns look very similar, which implies that convergence behavior in the V' and H_0^1 norms are essentially the same (in later tests we will only use V'). Overall, we see similar behavior in all tests. In all cases, AAg-Picard shows significant improvement over Picard, with AAg either dramatically accelerating convergence and even enabling it since Picard fails for $Re=150$ 2D channel flow past a block and both 3D cavity problems. We also observe that, except for the $Re=150$ 2D channel flow past a block tests, convergence is improved as the depth is increased.

In the third column of Figure 5, we observe in all cases that for larger enough k , γ_k agrees (essentially) exactly with the observed linear convergence ratio at each step. This suggests that our analysis is sharp: γ_k is a very good predictor of the linear convergence rate, once the higher order terms become negligible. Hence it fits that for the easier problems the agreement of $\frac{\|g(u_k)\|_{V'}}{\|g(u_{k-1})\|_{V'}}$ and γ_k is reached for smaller k , while for the harder problems they do not agree until k is much larger. We note that for classical AA, there is no known way to predict the linear convergence rate this accurately.

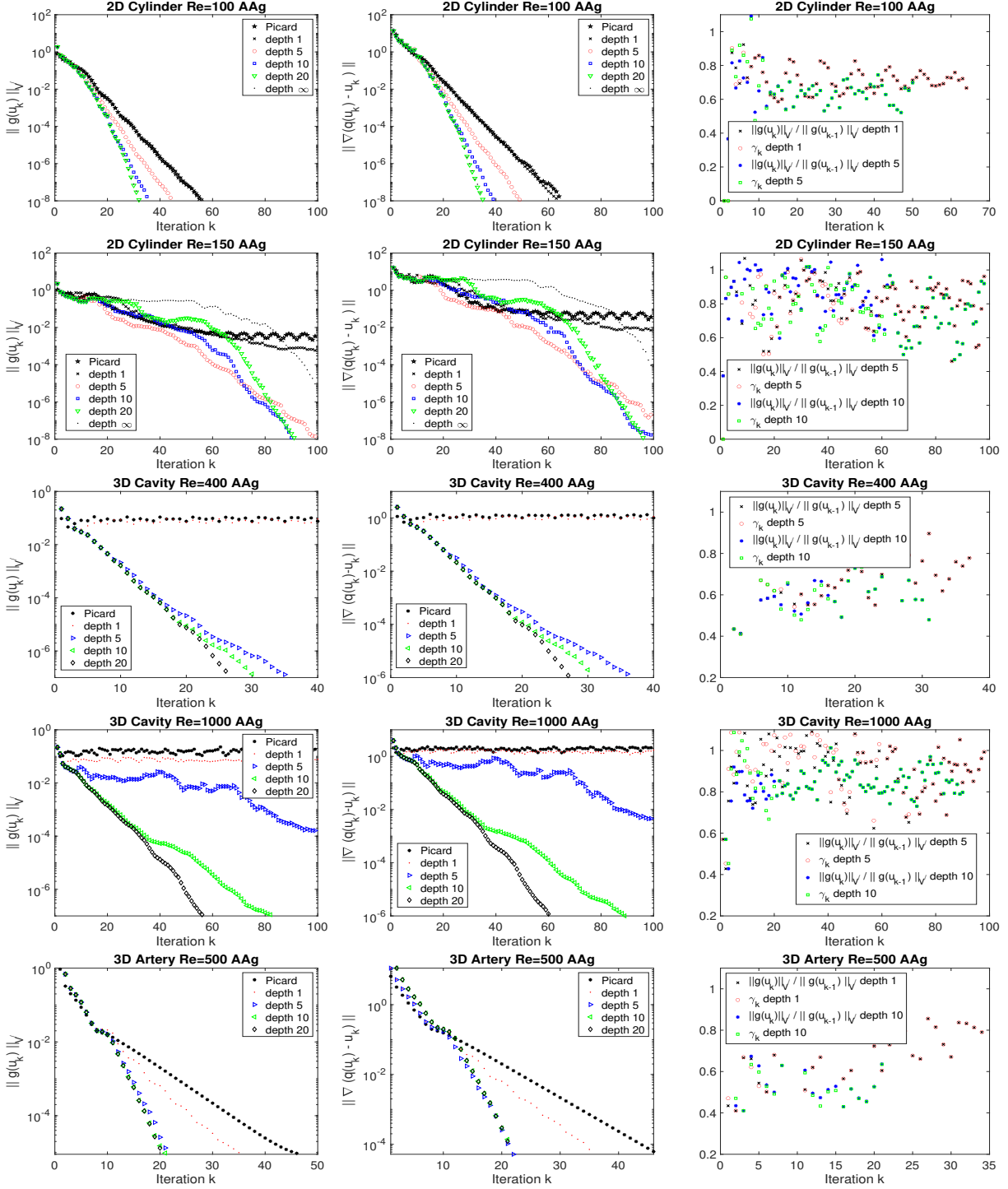


Figure 5: The plots above show AAg convergence in $\|g(u_k)\|_{V'}$, $\|\nabla(g(u_k) - u_k)\|$, and γ_k with $\frac{\|g(u_k)\|_{V'}}{\|g(u_{k-1})\|_{V'}}$ (left to right), for 2D channel flow past a block, 3D driven cavity, and 3D stenotic artery.

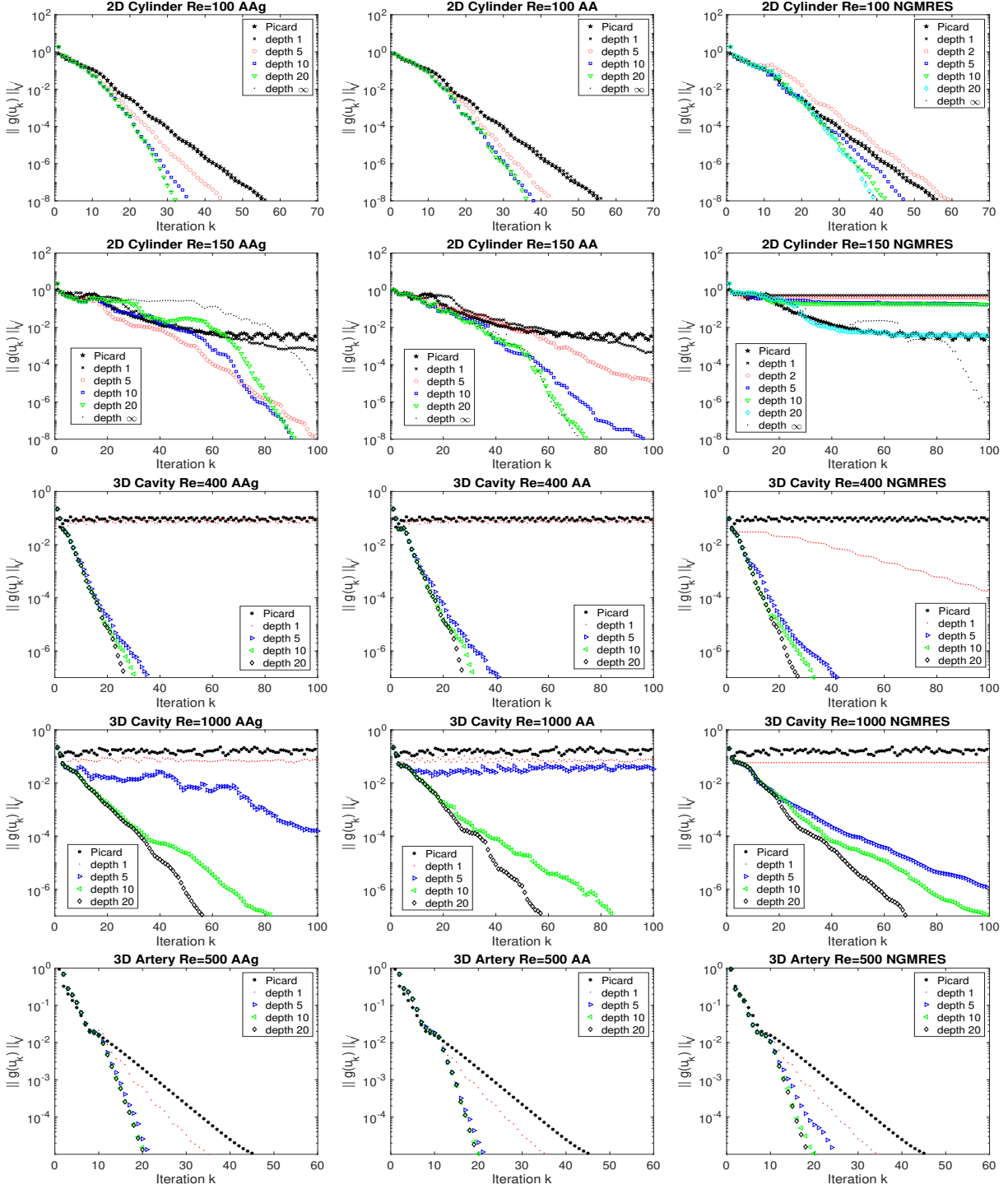


Figure 6: The plots above show convergence of AAg, AA and NGMRES (left to right) applied to Picard for the NSE for 2D flow past a block, 3D driven cavity, and 3D stenotic artery.

4.3 Convergence comparison for AAg, AA and NGMRES

For our next test, we compare convergence of AAg-Picard with AA-Picard and NGMRES-Picard, for each of the test problems. Convergence is compared using the V' norm, and various depths are used (noting that AA and AAg corresponds to $m = 1$, but NGMRES depth 1 corresponds to $m = 0$). The results are shown in Figure 6. Overall, we observe similar convergence behavior between the three methods. On 4 of the 5 tests (excluding $Re=150$ 2D channel flow past a block), AA-Picard and AAg-Picard are slightly better overall compared to NGMRES-Picard. But for $Re=150$ 2D channel flow past a block, AA-Picard and AAg-Picard perform much better than NGMRES-Picard; here, AA-Picard and AAg-Picard converge in under 100 iterations (or likely will soon after 100 iterations) for depths 5 and greater, while NGMRES-Picard never converges in under 100 iterations and only for depth ∞ does it appear that it will eventually converge.

In addition to convergence comparison, we also compare timings. Using AAg and NMGRES requires the optimization norm be the V' norm (as shown in [32], bad results are obtained in 3D if ℓ^2 is used instead). Unfortunately, to use the V' norm means that an additional Stokes solve needs performed at each iteration. Hence a cost comparison is in order, and we did this for each of our tests. For the 2D tests, a full LUPQ factorization (i.e. LU with row and column pivoting to minimize fill-in) of the Stokes matrix was performed at the start and reused throughout the computation. For 3D tests, an LUPQ factorization of the Stokes velocity block is saved, and the same type of Augmented Lagrangian solver as for the Picard solves is used for the Stokes solve. With these approaches, the extra Stokes solve adds roughly 20% to the total computational time for all of our tests (increase from about 6 seconds to nearly 8 seconds on average per iteration for the 2D block, and an increase from 16 to 19.5 seconds for the 3D cavity, on LR's workstation running Matlab 2023b with 196 GB RAM).

4.4 Adaptive depth with AAg-Picard

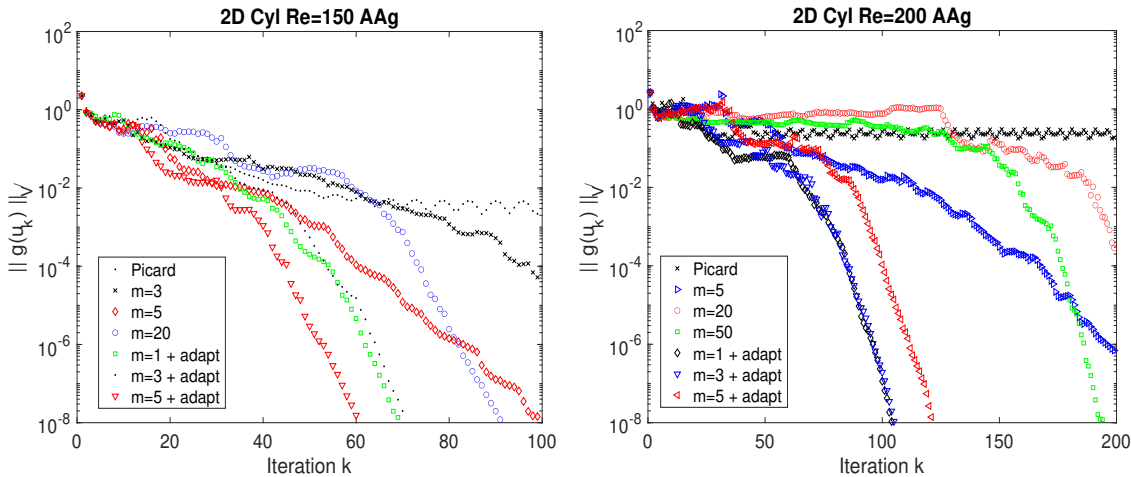


Figure 7: The plots above show convergence of AAg-Picard convergence for 2D channel flow past a block with $Re=150$ (left) and 200 (right), with varying constant depths and adaptive depths.

As observed in Theorem 3.2 and in numerical tests above, γ_k is a sharp predictor of the AAg Lipschitz constant, i.e. the linear convergence rate when the higher order terms do not play a role. This observation can be used to construct an adaptive strategy for choosing the depth m for AAg.

Theorem 3.2 shows that at iteration k , large m can be bad when u_{k-m+1} is far from the root. Hence while the iteration remains far from the root, using large m can hurt convergence. This is observed in the $Re=150$ 2D channel flow past a cylinder tests, where $m = \infty$ failed but smaller m performed better. This

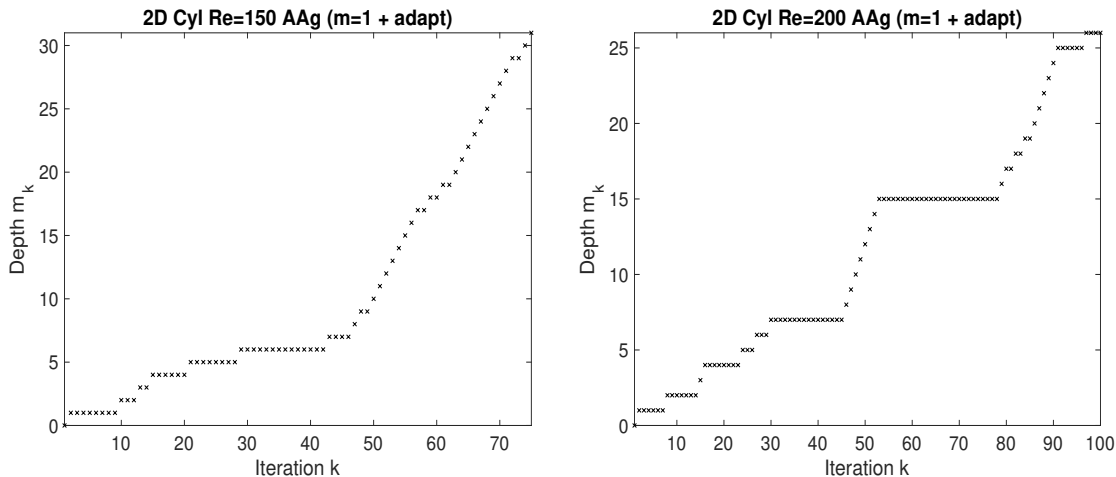


Figure 8: The plots above show the depths m_k used at iteration k for the AAg-Picard adaptive depth tests using $m = 1$ as the initial maximum depth, for 2D channel flow past a block with $Re=150$ (left) and 200 (right).

is also a well-known phenomena for AA-Picard for NSE, where the combination of small m early and larger m later in the iteration is shown to give better overall convergence [42].

One advantage AAg-Picard has over AA-Picard, however, is the sharp estimate γ_k of the Lipschitz constant. Under this, if one checks after step k that $\gamma_k \approx \frac{\|g(u_k)\|_{V'}}{\|g(u_{k-1})\|_{V'}}$, then the nonlinear terms are not playing a significant role in the convergence. Thus, when this happens, increasing m by 1 for the next iteration should help convergence by reducing the linear convergence rate contribution, but not allow the higher order terms to become significant and have a negative impact on convergence. In the tests below we checked if

$$\left| \gamma_k - \frac{\|g(u_k)\|_{V'}}{\|g(u_{k-1})\|_{V'}} \right| < 0.01,$$

then we increase m by 1.

We test this idea on 2D channel flow past a cylinder with $Re=150$ and 200, and results are shown in Figure 7 for AAg-Picard with varying constant depth m and adaptive depth that start with a small maximum $m=1, 3, 5$. We observe from the results that for $Re=150$, the adaptive depth computations perform much better than constant depths 3, 5, and 20 (recall from Figure 6 that $m = 20$ is the quasi-optimal depth). Of the three adaptive tests, using maximum $m = 5$ as the starting maximum gives the best results.

The success of the adaptive strategy is even clearer for the case of $Re=200$. Here, AAg-Picard with constant depths $m = 5$ and $m = 20$ fail, with $m = 50$ converging finally in 193 iterations. The adaptive depth tests with $m = 1$ and 3 as the initial maximum depth converge in 105 iterations, and the test with initial maximum of $m = 5$ converged in 122.

The depth m_k used at iteration k for the adaptive depth tests where $m = 1$ was the initial maximum depth are shown in Figure 8. We observe the general pattern of small m early in the iteration, and then large m later once the residual gets small. This is in agreement with our analysis results that larger m reduces the linear convergence rate but adds additional contributions from high order terms; when the residual is large, the higher order terms are not negligible and large m may not be advantageous. This is similar to what was found effective for usual AA [42] from a high level, but with AAg the better linear convergence rate prediction allows for a simple and very effective strategy.

5 Conclusions

In this work, we extend the AAg approach proposed in [29] to study its acceleration of the Picard iteration for the NSE. We present a convergence analysis for AAg with general depth that identifies the appropriate norm for the optimization problem and proves that AAg improves the linear convergence rate (and adds higher order terms). While usual AA also has a similar theory, the AAg has a distinct improvement in that the analysis provides a sharp prediction of the linear convergence at each step which can be used to develop adaptive depth strategies.

We present numerical results that illustrate our new convergence theory, and compare the performance of AAg, AA and NGMRES for both 2D and 3D problems. We observe similar convergence behavior between the three methods using constant depths, although for some tests NGMRES performed slightly worse. While AA and AAg have similar behavior with constant depths, AAg and NGMRES are somewhat more expensive at each iteration due to the extra Stokes solve needed for the optimization problem. Our tests also showed that a first attempt at an adaptive strategy based on γ_k yielded a strong improvement in performance over constant depth choices.

The new analysis of AAg and its use to develop adaptive depth strategies should be extended beyond the application of the Picard iteration for the NSE studied herein. Hence, next steps include extending our results to create a general theory for AAg, testing it on more applications including constraint optimization, and developing more sophisticated adaptive depth strategies.

6 Declarations

Funding: Author LR acknowledges funding support from the US Department of Energy grant DE-SC0025292.

Data Availability Statement: The datasets generated during and/or analyzed during the current study are available from the corresponding author on reasonable request.

Code Availability Statement: The computer codes used during the current study are available from the corresponding author on reasonable request.

References

- [1] H. An, X. Jia, and H. Walker. Anderson acceleration and application to the three-temperature energy equations. *Journal of Computational Physics*, 347:1–19, 2017.
- [2] D. G. Anderson. Iterative procedures for nonlinear integral equations. *J. Assoc. Comput. Mach.*, 12(4):547–560, 1965.
- [3] A. Z. Atanasov, B. Uekermann, C. Pachajoa, H. Bungartz, and P. Neumann. Steady-state Anderson accelerated coupling of Lattice Boltzmann and Navier-Stokes solvers. *Comput.*, 4:38, 2016.
- [4] N. A. Barnafi and M. L. Pasini. Two-level sketching alternating Anderson acceleration for complex physics applications. *arXiv preprint arXiv:2505.08587*, 2025.
- [5] M. Benzi and M. Olshanskii. An augmented Lagrangian-based approach to the Oseen problem. *SIAM J. Sci. Comput.*, 28:2095–2113, 2006.
- [6] W. Bian and X. Chen. Anderson acceleration for nonsmooth fixed point problems. *SIAM Journal on Numerical Analysis*, 60(5):2565–2591, 2022.
- [7] C. Brezinski, M. Redivo-Zaglia, and Y. Saad. Shanks sequence transformations and Anderson acceleration. *Siam Review*, 60(3):646–669, 2018.

- [8] P. N. Brown and Y. Saad. Hybrid Krylov methods for nonlinear systems of equations. *SIAM Journal on Scientific and Statistical Computing*, 11(3):450–481, 1990.
- [9] P. N. Brown and Y. Saad. Convergence theory of nonlinear Newton–Krylov algorithms. *SIAM Journal on Optimization*, 4(2):297–330, 1994.
- [10] P. R. Brune, M. G. Knepley, B. F. Smith, and X. Tu. Composing scalable nonlinear algebraic solvers. *siam REVIEW*, 57(4):535–565, 2015.
- [11] T. Charnyi, T. Heister, M. Olshanskii, and L. Rebholz. On conservation laws of Navier–Stokes Galerkin discretizations. *Journal of Computational Physics*, 337:289–308, 2017.
- [12] K. Chen and C. Vuik. Composite Anderson acceleration method with two window sizes and optimized damping. *International Journal for Numerical Methods in Engineering*, 123(23):5964–5985, 2022.
- [13] H. De Sterck. A nonlinear GMRES optimization algorithm for canonical tensor decomposition. *SIAM Journal on Scientific Computing*, 34(3):A1351–A1379, 2012.
- [14] H. De Sterck and Y. He. On the asymptotic linear convergence speed of Anderson acceleration, Nesterov acceleration, and nonlinear GMRES. *SIAM Journal on Scientific Computing*, 43(5):S21–S46, 2021.
- [15] C. Evans, S. Pollock, L. Rebholz, and M. Xiao. A proof that Anderson acceleration improves the convergence rate in linearly converging fixed-point methods (but not in those converging quadratically). *SIAM Journal on Numerical Analysis*, 58:788–810, 2020.
- [16] H. Fang and Y. Saad. Two classes of multiseccant methods for nonlinear acceleration. *Numer. Linear Algebra Appl.*, 16(3):197–221, 2009.
- [17] X. Feng, M. P. Laiu, and T. Strohmer. Convergence analysis of the alternating Anderson–Picard method for nonlinear fixed-point problems. *SIAM Journal on Scientific Computing*, pages S436–S461, 2025.
- [18] M. Filippini, P. Alotto, and A. Giust. Anderson acceleration for electromagnetic nonlinear problems. *Compel*, 38(5):1493–1506, 2019.
- [19] D. Forbes, L. G. Rebholz, and F. Xue. Anderson acceleration of nonlinear solvers for the stationary Gross-pitaevskii equation. *Advances in Applied Mathematics and Mechanics*, 13(5):1096–1125, 2021.
- [20] A. Fu, J. Zhang, and S. Boyd. Anderson accelerated Douglas–Rachford splitting. *SIAM Journal on Scientific Computing*, 42(6):A3560–A3583, 2020.
- [21] V. Girault and P.-A. Raviart. *Finite element methods for Navier–Stokes equations: Theory and algorithms*. Springer-Verlag, 1986.
- [22] C. Greif and Y. He. Convergence properties of nonlinear GMRES applied to linear systems. *SIAM Journal on Matrix Analysis and Applications*, 47(1):330–352, 2026.
- [23] W. W. Hager and H. Zhang. A survey of nonlinear conjugate gradient methods. *Pacific Journal of Optimization*, 2(1):35–58, 2006.
- [24] E. Hawkins and L. Rebholz. On the choice of optimization norm for Anderson acceleration of the Picard iteration for Navier–Stokes equations. *Numerical Methods for Partial Differential Equations*, in revision, 2026.
- [25] E. Hawkins, L. Rebholz, and D. Vargun. Removing splitting/modeling error in projection/penalty methods for Navier–Stokes simulations with continuous data assimilation. *Communications in Mathematical Research*, 40(1):1–29, 2024.

- [26] H. He, Z. Tang, S. Zhao, Y. Saad, and Y. Xi. nlTGCR: A class of nonlinear acceleration procedures based on conjugate residuals. *SIAM Journal on Matrix Analysis and Applications*, 45(1):712–743, 2024.
- [27] Y. He. Convergence analysis for nonlinear GMRES. *IMA Journal of Numerical Analysis*, 2026.
- [28] Y. He. Convergence analysis of an alternating nonlinear GMRES on linear systems. *Numerical Linear Algebra with Applications*, 33(1):e70065, 2026.
- [29] Y. He. Properties of nonlinear GMRES applied to the preconditioned Richardson iteration. *arXiv preprint arXiv:2603.25983*, 2026.
- [30] Y. He and S. Leveque. A generalized alternating Anderson acceleration method. *To appear, Journal of Scientific Computing*, 2026.
- [31] Y. He and A. Mang. A generalized alternating NGMRES method for PDE-constrained optimization problems governed by transport equations. *arXiv preprint arXiv:2510.08782*, 2025.
- [32] Y. He and L. Rebholz. Convergence analysis and proof of acceleration for NGMRES applied to the Picard iteration for Navier-Stokes equations. *submitted*, 2026.
- [33] T. Heister and G. Rapin. Efficient augmented Lagrangian-type preconditioning for the Oseen problem using grad-div stabilization. *Int. J. Numer. Meth. Fluids*, 71:118–134, 2013.
- [34] V. Henson et al. Multigrid methods nonlinear problems: an overview. *Computational Imaging*, 5016:36–48, 2003.
- [35] V. John, A. Linke, C. Merdon, M. Neilan, and L. G. Rebholz. On the divergence constraint in mixed finite element methods for incompressible flows. *SIAM Review*, 59(3):492–544, 2017.
- [36] W. Layton. *An Introduction to the Numerical Analysis of Viscous Incompressible Flows*. SIAM, Philadelphia, 2008.
- [37] M. Olshanskii and L. Rebholz. Approximating a branch of solutions to the Navier-Stokes equations by reduced-order modeling. *Journal of Computational Physics*, 524:1–14, 2025.
- [38] C. W. Oosterlee and T. Washio. Krylov subspace acceleration of nonlinear multigrid with application to recirculating flows. *SIAM Journal on Scientific Computing*, 21(5):1670–1690, 2000.
- [39] Y. Peng, B. Deng, J. Zhang, F. Geng, W. Qin, and L. Liu. Anderson acceleration for geometry optimization and physics simulation. *ACM Trans. Graph.*, 37(4), 2018.
- [40] S. Pollock and L. Rebholz. Anderson acceleration for contractive and noncontractive operators. *IMA Journal of Numerical Analysis*, 41(4):2841–2872, 2021.
- [41] S. Pollock and L. Rebholz. Filtering for Anderson acceleration. *SIAM Journal on Scientific Computing*, 45(4):A1571–A1590, 2023.
- [42] S. Pollock and L. Rebholz. *Anderson Acceleration for Numerical PDEs*. Society for Industrial and Applied Mathematics, Philadelphia, 2025.
- [43] S. Pollock, L. Rebholz, X. Tu, and M. Xiao. Analysis of the Picard-Newton iteration for the Navier-Stokes equations: global stability and quadratic convergence. *Journal of Scientific Computing*, 14(25):1–23, 2025.
- [44] S. Pollock, L. Rebholz, and M. Xiao. Anderson-accelerated convergence of Picard iterations for incompressible Navier-Stokes equations. *SIAM Journal on Numerical Analysis*, 57:615–637, 2019.

- [45] W. Rodi. Comparison of LES and RANS calculations of the flow around bluff bodies. *Journal of Wind Engineering and Industrial Aerodynamics*, 69-71:55–75, 1997. Proceedings of the 3rd International Colloquium on Bluff Body Aerodynamics and Applications.
- [46] Y. Saad. Acceleration methods for fixed-point iterations. *Acta Numerica*, 34:805–890, 2025.
- [47] A. Sohankar, L. Davidson, and C. Norberg. Large eddy simulation of flow past a square cylinder: Comparison of different subgrid scale models. *Journal of Fluids Engineering*, 122(1):39–47, 11 1999.
- [48] Z. Tang, T. Xu, H. He, Y. Saad, and Y. Xi. Anderson acceleration with truncated Gram–Schmidt. *SIAM Journal on Matrix Analysis and Applications*, 45(4):1850–1872, 2024.
- [49] R. Temam. *Navier-Stokes equations*. Elsevier, North-Holland, 1991.
- [50] J. M. Tempestti, S. Kim, B. Lindsey, and A. Veneziani. A pseudo-spectral method for wall shear stress estimation from Doppler ultrasound imaging in coronary arteries. *Cardiovascular Engineering and Technology*, 15(6):647–666, 2024.
- [51] A. Toth, C. Kelley, S. Slattery, S. Hamilton, K. Clarno, and R. Pawlowski. Analysis of Anderson acceleration on a simplified neutronics/thermal hydraulics system. *Proceedings of the ANS MC2015 Joint International Conference on Mathematics and Computation (M&C), Supercomputing in Nuclear Applications (SNA) and the Monte Carlo (MC) Method*, ANS MC2015 CD:1–12, 2015.
- [52] F. Trias, A. Gorobets, and A. Oliva. Turbulent flow around a square cylinder at Reynolds number 22,000: A DNS study. *Computers & Fluids*, 123:87–98, 2015.
- [53] H. F. Walker and P. Ni. Anderson acceleration for fixed-point iterations. *SIAM J. Numer. Anal.*, 49(4):1715–1735, 2011.
- [54] D. Wang, Y. He, and H. De Sterck. On the asymptotic linear convergence speed of Anderson acceleration applied to ADMM. *Journal of Scientific Computing*, 88(2):38, 2021.
- [55] Q. Wang, W. Li, W. Bao, and X. Gao. Nonlinear Kaczmarz algorithms and their convergence. *Journal of Computational and Applied Mathematics*, 399:113720, 2022.
- [56] T. Washio and C. W. Oosterlee. Krylov subspace acceleration for nonlinear multigrid schemes. *Electron. Trans. Numer. Anal.*, 6(271-290):3, 1997.
- [57] T. Werner, N. Wan, and A. Miedlar. nlkrylov: A unified framework for nonlinear GCR-type Krylov subspace methods. *arXiv preprint arXiv:2511.14713*, 2025.
- [58] D. Wicht, M. Schneider, and T. Bohlke. Anderson-accelerated polarization schemes for fast Fourier transform-based computational homogenization. *International Journal for Numerical Methods in Engineering*, 122(9):2287–2311, 2021.
- [59] K. Wong and A. Baker. A 3D incompressible Navier-Stokes velocity-vorticity weak form finite element algorithm. *International Journal for Numerical Methods in Fluids*, 38:99–123, 2002.
- [60] M. Xiao. Superlinear convergence of Anderson accelerated Newton’s method for solving stationary Navier-Stokes equations. *Numerical Methods for Partial Differential Equations*, 39:3089–3107, 2023.
- [61] Y. Yang. Anderson acceleration for seismic inversion. *Geophysics*, 86(1):R99–R108, 2021.

Appendix

In the Appendix, we give proofs of identities used in the analysis of Section 3.

Proof of Lemma 3.1. This proof uses the definition of u_{k+1} from AAg, that $\sum_{j=k-m+1}^{k+1} \alpha_j = 1$, and appropriately grouping terms. For the first identity, expanding u_{k+1} and using that $\sum_{j=k-m+1}^{k+1} \alpha_j = 1$, we get that

$$\begin{aligned} u_{k+1} - \tilde{u}_{k+1} &= -(1 - \alpha_{k+1})\tilde{u}_{k+1} + \alpha_k\tilde{u}_k + \dots + \alpha_{k-m+1}\tilde{u}_{k-m+1} \\ &= -(1 - \alpha_{k+1})\tilde{e}_{k+1} - (1 - \alpha_{k+1})\tilde{u}_k + \alpha_k\tilde{u}_k + \dots + \alpha_{k-m+1}\tilde{u}_{k-m+1} \\ &= \dots \\ &= -(1 - \alpha_{k+1})\tilde{e}_{k+1} - (1 - \alpha_{k+1} - \alpha_k)\tilde{e}_k - \dots - \alpha_{k-m+1}\tilde{e}_{k-m+2}, \end{aligned}$$

Similarly for the second and third identities,

$$\begin{aligned} u_{k+1} - \tilde{u}_k &= \alpha_{k+1}\tilde{u}_{k+1} - (1 - \alpha_k)\tilde{u}_k + \dots + \alpha_{k-m+1}\tilde{u}_{k-m+1} \\ &= \alpha_{k+1}\tilde{e}_{k+1} - (1 - \alpha_{k+1} - \alpha_k)\tilde{u}_k + \alpha_{k-1}\tilde{u}_{k-1} \dots + \alpha_{k-m+1}\tilde{u}_{k-m+1} \\ &= \alpha_{k+1}\tilde{e}_{k+1} - (1 - \alpha_{k+1} - \alpha_k)\tilde{e}_k - (1 - \alpha_{k+1} - \alpha_k - \alpha_{k-1})\tilde{u}_{k-1} \\ &\quad + \alpha_{k-2}\tilde{u}_{k-2} \dots + \alpha_{k-m+1}\tilde{u}_{k-m+1} \\ &= \dots \\ &= \alpha_{k+1}\tilde{e}_{k+1} - (1 - \alpha_{k+1} - \alpha_k)\tilde{e}_k - (1 - \alpha_{k+1} - \alpha_k - \alpha_{k-1})\tilde{e}_{k-1} \\ &\quad - \dots - \alpha_{k-m+1}\tilde{e}_{k-m+2} \end{aligned}$$

$$\begin{aligned} u_{k+1} - \tilde{u}_{k-1} &= \alpha_{k+1}\tilde{u}_{k+1} + \alpha_k\tilde{u}_k - (1 - \alpha_{k-1})\tilde{u}_{k-1} + \alpha_{k-2}\tilde{u}_{k-2} + \dots + \alpha_{k-m+1}\tilde{u}_{k-m+1} \\ &= \alpha_{k+1}\tilde{e}_{k+1} + (\alpha_{k+1} + \alpha_k)\tilde{u}_k - (1 - \alpha_{k-1})\tilde{u}_{k-1} + \alpha_{k-2}\tilde{u}_{k-2} + \dots + \alpha_{k-m+1}\tilde{u}_{k-m+1} \\ &= \alpha_{k+1}\tilde{e}_{k+1} + (\alpha_{k+1} + \alpha_k)\tilde{e}_k - (1 - \alpha_{k+1} - \alpha_k - \alpha_{k-1})\tilde{u}_{k-1} + \alpha_{k-2}\tilde{u}_{k-2} \\ &\quad + \dots + \alpha_{k-m+1}\tilde{u}_{k-m+1} \\ &= \dots \\ &= \alpha_{k+1}\tilde{e}_{k+1} + (\alpha_{k+1} + \alpha_k)\tilde{e}_k - (1 - \alpha_{k+1} - \alpha_k - \alpha_{k-1})\tilde{e}_{k-1} \\ &\quad - \dots - \alpha_{k-m+1}\tilde{e}_{k-m+2} \end{aligned}$$

This same process can be repeated for general $j < k$ via

$$\begin{aligned} u_{k+1} - \tilde{u}_j &= \alpha_{k+1}\tilde{e}_{k+1} + (\alpha_{k+1} + \alpha_k)\tilde{e}_k + \dots + (\alpha_{k+1} + \alpha_k + \dots + \alpha_{j+1})\tilde{e}_{j+1} \\ &\quad (1 - \alpha_{k+1} - \dots - \alpha_j)\tilde{e}_j - \dots - \alpha_{k-m+1}\tilde{e}_{k-m+2} \end{aligned}$$

□

We now establish (24). This result is simply an identity, although a long one, for which we use nothing more than definitions, expansions, and Lemma 3.1. Below, for simplicity of notation, equality is meant in the V' sense, i.e. weakly when tested with an arbitrary function from V .

Expanding u_{k+1} and using that $\sum_{j=k-m+1}^{k+1} \alpha_j = 1$ we obtain

$$\begin{aligned} g(u_{k+1}) &= u_{k+1} \cdot \nabla u_{k+1} - \nu \Delta u_{k+1} - f \\ &= \alpha_{k+1} (u_{k+1} \cdot \nabla \tilde{u}_{k+1} - \nu \Delta \tilde{u}_{k+1} - f) + \alpha_k (u_{k+1} \cdot \nabla \tilde{u}_k - \nu \Delta \tilde{u}_k - f) \\ &\quad + \dots + \alpha_{k-m+1} (u_{k+1} \cdot \nabla \tilde{u}_{k-m+1} - \nu \Delta \tilde{u}_{k-m+1} - f) \\ &= \alpha_{k+1} g(\tilde{u}_{k+1}) + \alpha_k g(\tilde{u}_k) + \dots + \alpha_{k-m+1} g(\tilde{u}_{k-m+1}) + \alpha_{k+1} (u_{k+1} - \tilde{u}_{k+1}) \cdot \nabla \tilde{u}_{k+1} \\ &\quad + \alpha_k (u_{k+1} - \tilde{u}_k) \cdot \nabla \tilde{u}_k + \dots + \alpha_{k-m+1} (u_{k+1} - \tilde{u}_{k-m+1}) \cdot \nabla \tilde{u}_{k-m+1}. \end{aligned}$$

Hence we can write

$$g(u_{k+1}) = \alpha_{k+1}g(\tilde{u}_{k+1}) + \alpha_k g(\tilde{u}_k) + \dots + \alpha_{k-m+1}g(\tilde{u}_{k-m+1}) + R, \quad (28)$$

where

$$R = \alpha_{k+1}(u_{k+1} - \tilde{u}_{k+1}) \cdot \nabla \tilde{u}_{k+1} + \alpha_k(u_{k+1} - \tilde{u}_k) \cdot \nabla \tilde{u}_k + \dots + \alpha_{k-m+1}(u_{k+1} - \tilde{u}_{k-m+1}) \cdot \nabla \tilde{u}_{k-m+1}.$$

We now analyze R further. Using Lemma 3.1 gives

$$\begin{aligned} R = & \alpha_{k+1} \left(- (1 - \alpha_{k+1})\tilde{e}_{k+1} - (1 - \alpha_{k+1} - \alpha_k)\tilde{e}_k - \dots - \alpha_{k-m+1}\tilde{e}_{k-m+2} \right) \cdot \nabla \tilde{u}_{k+1} \\ & + \alpha_k \left(\alpha_{k+1}\tilde{e}_{k+1} - (1 - \alpha_{k+1} - \alpha_k)\tilde{e}_k - (1 - \alpha_{k+1} - \alpha_k - \alpha_{k-1})\tilde{e}_{k-1} \right. \\ & \quad \left. - \dots - \alpha_{k-m+1}\tilde{e}_{k-m+2} \right) \cdot \nabla \tilde{u}_k \\ & + \alpha_{k-1} \left(\alpha_{k+1}\tilde{e}_{k+1} + (\alpha_{k+1} + \alpha_k)\tilde{e}_k - (1 - \alpha_{k+1} - \alpha_k - \alpha_{k-1})\tilde{e}_{k-1} \right. \\ & \quad \left. - \dots - \alpha_{k-m+1}\tilde{e}_{k-m+2} \right) \cdot \nabla \tilde{u}_{k-1} \\ & + \alpha_j \left(\alpha_{k+1}\tilde{e}_{k+1} + (\alpha_{k+1} + \alpha_k)\tilde{e}_k + \dots + (\alpha_{k+1} + \alpha_k + \dots + \alpha_{j+1})\tilde{e}_{j+1} + (1 - \alpha_{k+1} \right. \\ & \quad \left. - \dots - \alpha_j)\tilde{e}_j - \dots - \alpha_{k-m+1}\tilde{e}_{k-m+2} \right) \cdot \nabla \tilde{u}_j \\ & + \dots \\ & + \alpha_{k-m+1} \left(\alpha_{k+1}\tilde{e}_{k+1} + (\alpha_{k+1} + \alpha_k)\tilde{e}_k + \dots + (\alpha_{k+1} + \alpha_k + \dots + \alpha_j)\tilde{e}_j + \dots + \alpha_{k-m+1}\tilde{e}_{k-m+2} \right) \cdot \nabla \tilde{u}_{k-m+1}. \end{aligned}$$

The terms containing a \tilde{e}_{k+1} are as follows:

$$\begin{aligned} & \alpha_{k+1}\tilde{e}_{k+1} \cdot \nabla \left(- (1 - \alpha_{k+1})\tilde{u}_{k+1} + \alpha_k\tilde{u}_k + \alpha_{k-1}\tilde{u}_{k-1} + \dots + \alpha_{k-m+1}\tilde{u}_{k-m+1} \right) \\ & = \alpha_{k+1}\tilde{e}_{k+1} \cdot \nabla(u_{k+1} - \tilde{u}_{k+1}). \end{aligned}$$

The terms containing a \tilde{e}_k are as follows:

$$\begin{aligned} & \tilde{e}_k \cdot \nabla(-\alpha_{k+1}\tilde{u}_{k+1} - \alpha_k\tilde{u}_k) + (\alpha_k + \alpha_{k+1})\tilde{e}_k \cdot \nabla \left(\alpha_{k+1}\tilde{u}_{k+1} + \dots + \alpha_{k-m+1}\tilde{u}_{k-m+1} \right) \\ & = \tilde{e}_k \cdot \nabla(-\alpha_{k+1}\tilde{u}_{k+1} - \alpha_k\tilde{u}_k) + (\alpha_k + \alpha_{k+1})\tilde{e}_k \cdot \nabla u_{k+1} \\ & = \alpha_k\tilde{e}_k \cdot \nabla(u_{k+1} - \tilde{u}_k) + \alpha_{k+1}\tilde{e}_k \cdot \nabla(u_{k+1} - \tilde{u}_{k+1}). \end{aligned}$$

Similarly, the terms with \tilde{e}_j reduce to

$$\sum_{i=j}^{k+1} \alpha_i \tilde{e}_j \cdot \nabla(u_{k+1} - \tilde{u}_i).$$

We can now write R as

$$R = \sum_{j=k-m+2}^{k+1} \sum_{i=j}^{k+1} \alpha_i \tilde{e}_j \cdot \nabla(u_{k+1} - \tilde{u}_i). \quad (29)$$